

# Preparation and Application of Polyaluminum Ferric Sulfate from Red Mud: Behaviors of Leaching, Polymerizing, and Coagulation

Wang Li,\* Panpan Zhang, and Xiaobo Zhu\*

Cite This: *ACS Omega* 2024, 9, 2468–2479

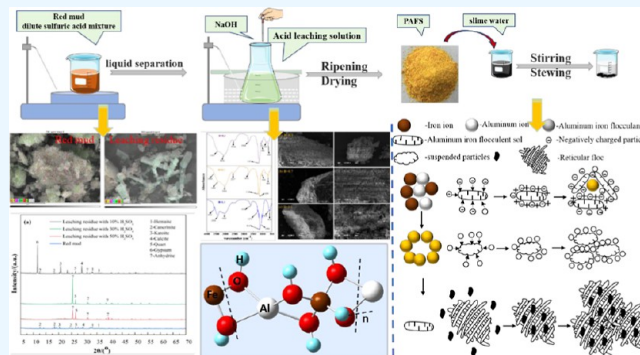
Read Online

ACCESS |

Metrics &amp; More

Article Recommendations

**ABSTRACT:** Red mud is a solid waste containing valuable components, such as aluminum and iron. This paper aims to recover aluminum and iron from red mud by acid leaching and prepare polyaluminum ferric sulfate (PAFS) to apply for the turbidity reduction treatment of coal slurry water. The behaviors of leaching, polymerizing, and coagulation were analyzed by leaching thermodynamics and advanced micro-detection methods. More than 90% of aluminum and 60% of iron in red mud were dissolved into the leaching solution by using 50% sulfuric acid (v/v) with 7 mL/g at 100 °C for 2 h, where the crystal lattice of cancrinite was significantly destroyed to promote the dissolution of aluminum. The low polymerization (Al + Fe)<sub>a</sub>, medium polymerization (Al + Fe)<sub>b</sub>, and high polymerization (Al + Fe)<sub>c</sub> could be generated in PAFS by adjusting the basicity of the leaching solution with 0.7–0.9. The removal efficiency of turbidity of wastewater could reach more than 95% by using PAFS at 25 mg/L in the pH range of 6.0–7.0. The turbidity reduction mechanism included not only the electric neutralization of (Al + Fe)<sub>a</sub> but also the adsorption of (Al + Fe)<sub>b</sub> and the entrapment effect of (Al + Fe)<sub>c</sub>. This current study contributes to the future development of red mud based on flocculants containing aluminum and iron for wastewater treatment.



## 1. INTRODUCTION

Red mud is the residue of aluminum smelting from bauxite, which has a strong alkalinity.<sup>1</sup> The weathering of red mud particles in the exposed environment easily causes air pollution. Furthermore, the strong alkalinity of red mud will erode the building surface, alkalinize the soil, and affect the planting. The red mud dump can produce strong alkaline leachate, which can also harm people and animals near the dump.<sup>2</sup> Therefore, many researchers have used red mud, fly ash, and coal gangue to prepare geopolymers and roadbed materials and achieved some good application results.<sup>3,4</sup> However, it is worth noting that the red mud contains many available chemical components such as aluminum, iron, and scandium, in which the content of aluminum and iron accounts for 40–60% of the total amount.<sup>5,6</sup> Efficient recovery of aluminum and iron from red mud is an important way for its comprehensive utilization of “reduction, recycling, and harmlessness”. At present, the extraction of aluminum and iron from red mud mainly involves magnetization roasting-magnetic separation for the recovery of iron and alkali roasting-alkali leaching for the recovery of aluminum. However, the comprehensive recovery of aluminum and iron and the preparation of aluminum–iron inorganic flocculants have certain research significance.

The deterioration of water quality is becoming more and more serious with rapid economic growth. The traditional process of wastewater treatment cannot ensure a qualified and

safe effluent.<sup>7,8</sup> The addition of flocculants is a key step in the wastewater treatment process, among which inorganic flocculants have been widely used due to their simple preparation and convenient use.<sup>9,10</sup> So far, many researchers have proposed a variety of inorganic polymer flocculants, such as polyaluminum chloride, polyaluminum sulfate, polyaluminum phosphate, polyaluminum ferric silicate (PAFSi), polyaluminum silicate, and other inorganic polymer flocculants, as well as polyaluminum composite flocculants doped with organic polymers.<sup>11–17</sup> With the development of the times, many researchers began to prepare the flocculant of PAF by using some solid wastes.<sup>18–22</sup> The principle of this method is to extract the iron, aluminum, and silicon into a leaching solution from the solid wastes, and then, the leaching solution could react and polymerize under certain conditions. The investigations have achieved great success; for example, Ding et al. studied the preparation of high-efficiency coagulant PAFCaC with coal gangue as a raw material, which was used

Received: September 14, 2023

Revised: November 9, 2023

Accepted: December 12, 2023

Published: January 3, 2024



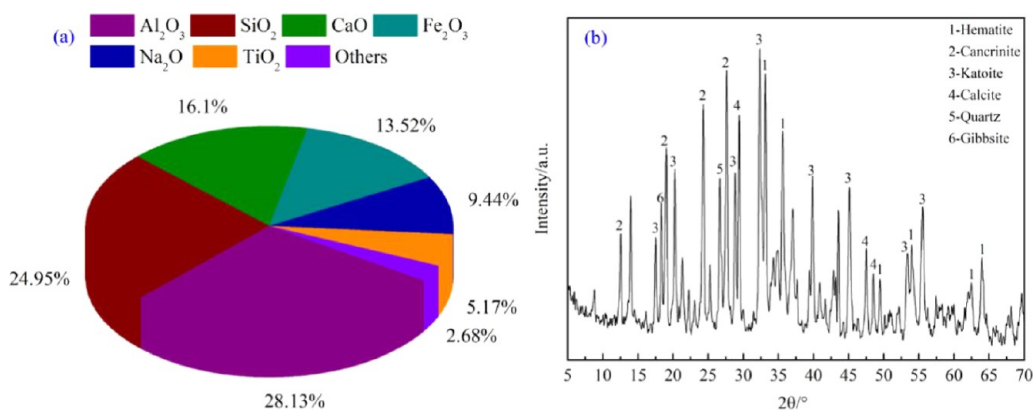


**Figure 1.** Main chemical composition (a) and mineral composition (b) of red mud.

to treat industrial wastewater. Compared with the traditional aluminum sulfate coagulant, it had the advantages of a lower dosage, no toxicity, and good floc sedimentation performance.<sup>23</sup> Gao et al. prepared a new coagulant of PAFSi with fly ash and pyrite slag to treat the wastewater of carton factory and domestic sewage. The treatment effect of COD was better than that of commercially available coagulants of PAC and PFC.<sup>24</sup> Regarding the preparation of flocculants with red mud, some scholars have proposed that the red mud was leached with hydrochloric acid, sulfuric acid, etc. Then, the aging and drying of the acid-leaching solution were carried out to prepare the polymeric aluminum–iron flocculant.<sup>25,26</sup> The flocculant has been applied to the removal of turbidity, such as kaolin, in which a good removal rate of more than 85% was achieved. However, the dissolution performance differences of aluminum, iron, and other components in the leaching, as well as the polymerization migration behavior, can significantly affect the morphology and application effect of the aluminum–iron flocculant. Furthermore, the reduction mechanism of turbidity on wastewater using the aluminum–iron flocculant was still unclear.

Therefore, comprehensive experiments and theoretical analysis were carried out to study the leaching of aluminum and iron from red mud with sulfuric acid. Instruments such as infrared spectroscopy and scanning electron microscopy (SEM) were used to elucidate the micromorphology and migration behavior of aluminum–iron polymerization products. Zeta potential and SEM were used to analyze the action mechanism of the aluminum–iron flocculant in the coagulation process of coal slurry wastewater. This investigation will provide some new ideas for the efficient recovery of aluminum and iron from red mud. Furthermore, the study can promote the controllable preparation of PAFS based on red mud and its efficient coagulation application for wastewater treatment.

## 2. MATERIALS AND METHODS

**2.1. Materials.** The red mud sample was collected from the Henan Province, and its chemical composition and phase analysis were detected with inductively coupled plasma-atomic emission spectrometry (ICP-AES) and X-ray diffraction (XRD), respectively (see Figure 1).

Figure 1 shows that the red mud sample contained a large amount of Al<sub>2</sub>O<sub>3</sub> (28.13%), SiO<sub>2</sub> (24.95%), CaO (16.1%), and Fe<sub>2</sub>O<sub>3</sub> (13.52%), which was similar to that of red mud described in the literature.<sup>27</sup> The aluminum and iron had a high content and an important recycling value. In addition, the

content of Na<sub>2</sub>O (9.44%) was also high as a typical strong alkaline solid waste. Aluminum and sodium were mainly present in cancrinite; however, iron was mainly present in hematite, and calcium mainly existed in cancrinite and calcite. The crystal lattice of these minerals was usually stable and difficult to destroy, so acid leaching was needed to destroy the crystal lattice and dissolve aluminum and iron.<sup>28</sup>

The reagents including H<sub>2</sub>SO<sub>4</sub> and NaOH with analytical grade were used in this study. The deionized water was prepared for the aqueous solutions and standard solutions.

**2.2. Preparation of PAFS.** A red mud of 50 g was mixed into the sulfuric acid solution with different concentrations (i.e., 10, 20, 30, 40, and 50%) at different liquid-to-solid ratios (i.e., 3, 5, 7, 9, and 11 mL/g) in a beaker. Then, the ore pulp was stirred at different leaching temperatures (i.e., 40, 60, 80, 100, and 120 °C) for a period of time (i.e., 0.5, 1, 1.5, 2, and 2.5 h). The acid-leaching solution was obtained after stirring by solid–liquid separation with a suction filter. Next, a NaOH solution of 3 mol/L was extremely slowly added into the acid leaching solution to obtain different basicities (i.e., 0.3, 0.5, 0.7, 0.9, and 1.1). The flocculant of PAFS was obtained by stirring for 1 h. The degree of polymerization increased with aging for 24 h at 25 °C. Finally, the thick liquid flocculant was dried three times at 60 °C to obtain the powder of PAFS.

**2.3. Application of PAFS.** The experiments were carried out on a magnetic stirrer (ZNCL-TS, YUHUA Scientific Instrument, Gongyi, China). The slime water of 100 mL was poured into a beaker, and then some PAFS (i.e., 5, 10, 15, 20, 25, 30, 35, and 40 mg/L) was added into the beaker. The mixture was adjusted to the pH value (i.e., 2, 3, 4, 5, 6, 7, 8, 9, and 10) and stirred at 300 rpm for 2 min. Then, the mixture was coagulated slowly at 80 rpm for 8 min and settled for 10 min. The turbidimeter (WGZ-1A, LICHEN Scientific Instrument, Shanghai, China) was used to measure the residual turbidity of water samples. Also, the chrominance of water samples was determined by a UV spectrophotometer (UV-1700, Macy, Shanghai, China).

**2.4. Analysis Methods.** **2.4.1. Chemical Properties and Micromorphology of PAFS.** The pH values of the solution were measured by a pH meter (PHS-3C, YOKE Scientific Instrument, Shanghai, China). The concentrations of Fe<sup>3+</sup> and Al<sup>3+</sup> were determined by a UV spectrophotometer (UV-1700, Macy, Shanghai, China). The phase compositions of products were confirmed by XRD (Smart Lab (9 kW), Japan). The functional groups of products were characterized by an FT-IR spectrophotometer (FT-IR, PerkinElmer Frontier, USA). The

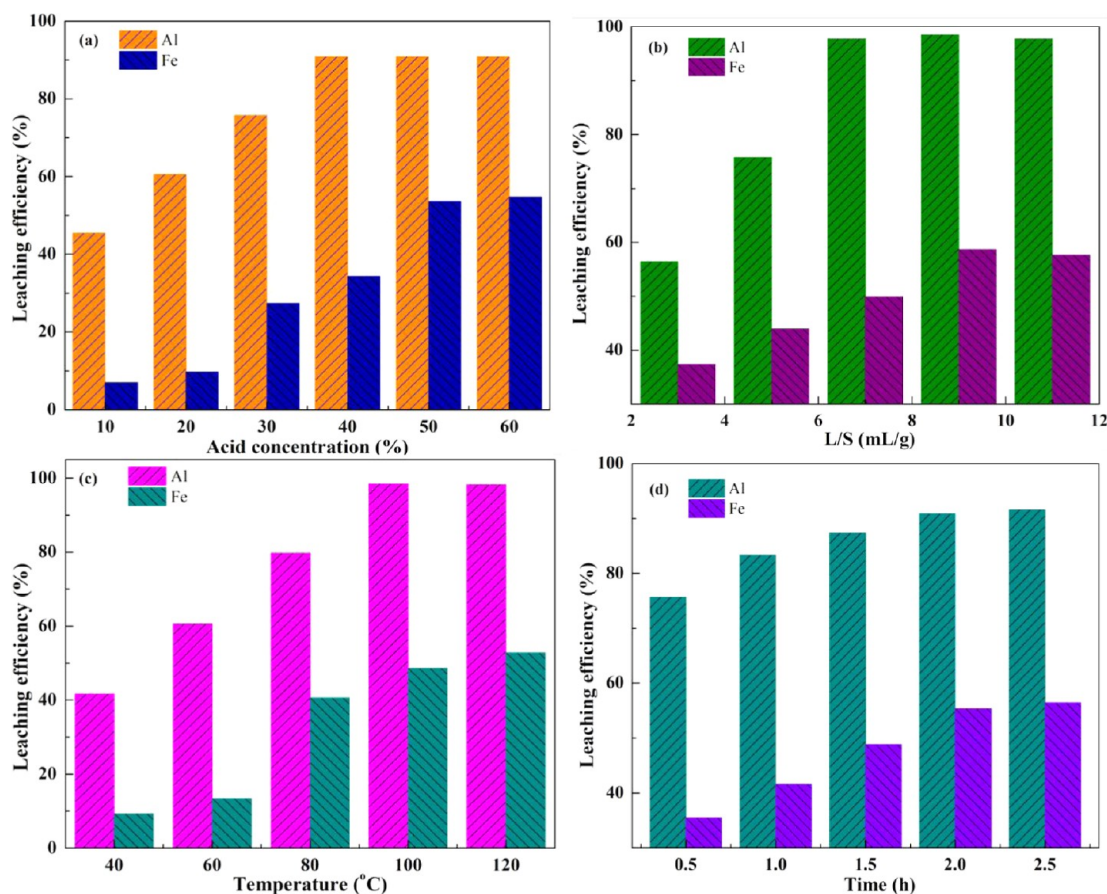


**Figure 2.** Parameter influence of sulfuric acid leaching to extract aluminum and iron from red mud: (a) sulfuric acid concentration, (b) liquid-to-solid ratio, (c) leaching temperature, and (d) reaction time.

morphologies of the products and the composition of the corresponding test position were investigated by SEM coupled with energy-dispersive X-ray spectroscopy (SEM-EDS, Merlin Compact, Germany).

**2.4.2. Species Distribution Analysis of Al and Fe.** The method of Ferron complexation-timed spectrophotometry was applied to distinguish the aqueous species of Al and Fe. The amounts of the Al–Ferron complex and Fe–Ferron complex were determined with the visible light absorbance at 370 and 597 nm, respectively. The monomer ( $Al_a$ ) and polymer ( $Al_b$ ) were analyzed by visible light absorption at 390 nm for 1 and 120 min, respectively.  $Al_a$  and  $Al_b$  were subtracted from the known total aluminum concentration to obtain the precipitated species ( $Al_c$ ). The species of Fe(III) were determined with the similar method above at a visible light absorbance of 597 nm.

### 3. RESULTS AND DISCUSSION

#### 3.1. Recovery of Al and Fe from Red Mud with $H_2SO_4$ .

**3.1.1. Influence of Leaching Parameters.** The effects of leaching parameters on the recovery of aluminum and iron from red mud were studied (see Figure 2).

Figure 2a indicates that the change of the acid concentration significantly affected the leaching effect of aluminum and iron. The recovery of Al and Fe showed first increasing and then flattening out with an increase of sulfuric acid concentration. The recovery of Al was from 44 to 92% with increasing sulfuric acid concentration from 10 to 40%. The aluminum in red mud mainly existed in cancrinite, which belonged to a silicate aluminate mineral. The increase of sulfuric acid concentration

was beneficial for destroying the mineral lattice of cancrinite, which could promote the effective progress of the acid–base reaction and improve the leaching efficiency of aluminum.<sup>29,30</sup> Under the same conditions, the recovery of Fe only increased from 7 to 34%. The iron in red mud mainly existed in hematite, where its lattice energy was large and its reaction activity was poor, resulting in the low leaching efficiency. Therefore, a suitable sulfuric acid concentration of 50% was chosen. Figure 2b shows that the effect of the liquid/solid ratio (L/S) on the recovery of Al could be divided into two stages. The first stage was an L/S ratio of 3–7, where the recovery of Al increased from 57% to over 92%. The L/S ratio could affect the contact between the two phases, where an increase of L/S would promote the diffusion of the liquid phase toward the interior of the particles and accelerate the destruction of the lattice of red mud minerals.<sup>31</sup> The second stage was an L/S ratio of 7–11, in which the recovery growth trend of Al was slight. The leaching trend of Fe was similar to that of Al, but its highest recovery still did not exceed 60%. The viscosity of the reaction system decreased with an increase of L/S, where the mass transfer resistance reduced and the recovery of Al and Fe increased.<sup>32</sup> While the L/S ratio was greater than 9, a further increase of L/S could lead to a decrease of the hydrogen ion concentration. The decrease of activity and reaction rate resulted in a slight decrease in the recovery of Al and Fe; therefore, an L/S ratio of 7 mL/g was more appropriate. Figure 2c shows that the leaching temperature can significantly affect the recovery of Al and Fe. The recovery of Al and Fe first increased and then tended to flatten out with an increase of the

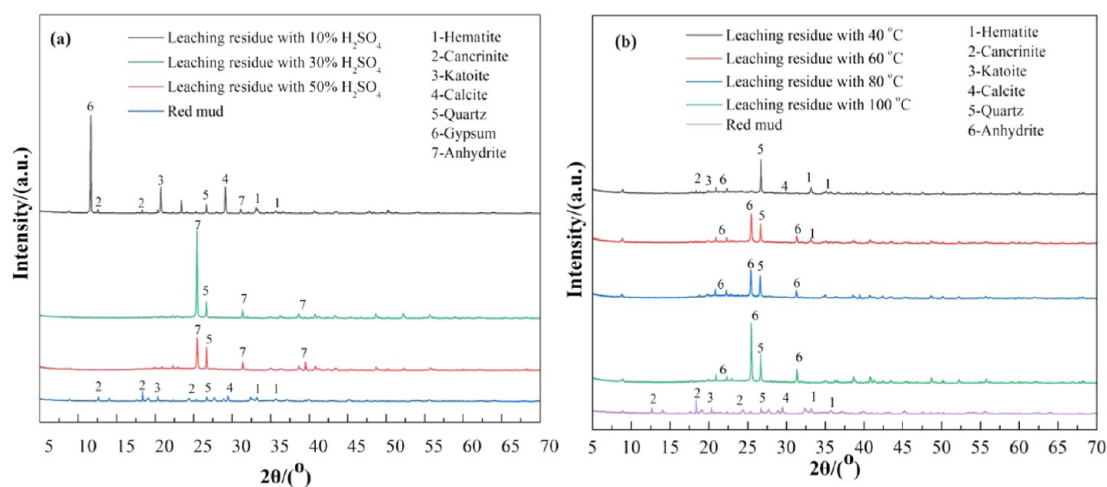


**Figure 3.** XRD phase of the leaching residue with different sulfuric acid concentrations (a) and leaching temperatures (b).

leaching temperature. The recovery of Al increased from 40 to 92% with increasing temperature from 40 to 100 °C, whereas the recovery of Fe increased from 8 to 50%. The increase of leaching temperature could increase the reactivity of sulfuric acid and accelerate the destruction of the mineral lattice and the reaction rate.<sup>33</sup> It was conducive to the diffusion of reaction molecules and chemical reactions. According to the perspective of leaching kinetics, the diffusion of the sulfuric acid solution into the red mud particles was also accelerated with increasing temperature.<sup>2</sup> Therefore, a suitable leaching temperature of 100 °C was chosen. Figure 2d shows that the influence of time on the recovery of Al and Fe was different. The recovery of Al increased from 78 to 92% with increasing time from 0.5 to 2 h, while the recovery of Fe increased from 33 to 55%. It indicates that the aluminum-bearing mineral cancrinite in red mud reacted violently in a short time (30 min), resulting in a high recovery of Al. Reaction time was the guarantee for ensuring the full progress of chemical reactions and reaching the equilibrium state. Especially for the two-phase stirring reactions between solid and liquid, it needed to take a certain time to complete the corresponding physical and chemical reactions.<sup>34</sup> The leaching process of hematite needed a long time, which may be related to the poor solubility of hematite in sulfuric acid.<sup>2</sup> Therefore, a leaching time of 2 h was suitable.

**3.1.2. Changes in the Morphology, Composition, and Phase of Leaching Residues.** The above research indicates that sulfuric acid concentration and temperature were the main factors in the recovery of Al and Fe. Therefore, the phase changes and microscopic morphology changes of the leaching residue under different concentrations of sulfuric acid and temperatures were analyzed. The results are shown in Figures 3 and 4, respectively.

Figure 3 shows that the phase diffraction peaks in the original red mud disappeared or weakened and that some new phase diffraction peaks appeared in the leaching residue. It indicates that a series of reactions occurred during the acid-leaching process. The diffraction peaks of calcite, hematite, and cancrinite all existed in the leaching residue with 10% sulfuric acid (Figure 3a), indicating that iron, aluminum, calcium, and other oxides do not react completely with sulfuric acid. The diffraction peak of gypsum was formed in the leaching residue with 10% sulfuric acid, where the low concentration of sulfuric acid and high water content in the leaching system led to the crystallization formation of gypsum with water. The diffraction

peaks of calcite, hematite, and cancrinite gradually decreased until the diffraction peaks of calcite disappeared with increasing sulfuric acid concentration. The diffraction peaks of anhydrite were obvious, which indicates that the calcium carbonate has almost all reacted with sulfuric acid to generate calcium sulfate. The diffraction peak of cancrinite was weakened, while the diffraction peak of quartz was obvious. It indicates that the mineral lattice of cancrinite was damaged, in which the oxides of aluminum, calcium, and sodium reacted with sulfuric acid, but the dioxide of silicon did not react and remained in the leaching residue. The diffraction peak of hematite was weakened to a certain extent, which indicates that the oxide of iron could insufficiently react with sulfuric acid. Due to the weak reactivity between hematite and sulfuric acid, the leaching process required higher temperature and pressure conditions to fully react. However, it was more easily soluble in hydrochloric acid solution systems according to the literature.<sup>2</sup> The phase analysis results at different acid-leaching temperatures (Figure 3b) show that the phase diffraction peaks in the original red mud gradually decreased or even disappeared with increasing temperature, but the diffraction peaks of anhydrite and quartz in the leaching residue were significant. The leaching temperature was crucial for improving the reaction activity of sulfuric acid and its diffusion into the mineral particles. The increase of the leaching temperature could cause the leaching agent to damage the mineral lattice and promote chemical reactions.<sup>35</sup>

Figure 4 shows that the red mud was mainly composed of granular and layered particles with the structures embedded in each other, in which the surface of the red mud particles was relatively dense. After acid leaching by sulfuric acid with different concentrations (10, 30, and 50%) and leaching temperatures (40, 60, 80, and 100 °C), the original sheet-like structure of red mud decreased or even disappeared, while more small loose particles were generated. Furthermore, the irregular cluster substances in the original red mud almost disappeared, and the main part was composed of divergent rod-shaped and small particles. It indicates that the main structure of red mud was severely corroded and the surface was heavily etched in the acid-leaching process. The morphology changes of the leaching residue of red mud were consistent with those of different solid materials with acid leaching in existing literature. While the acid concentration, leaching

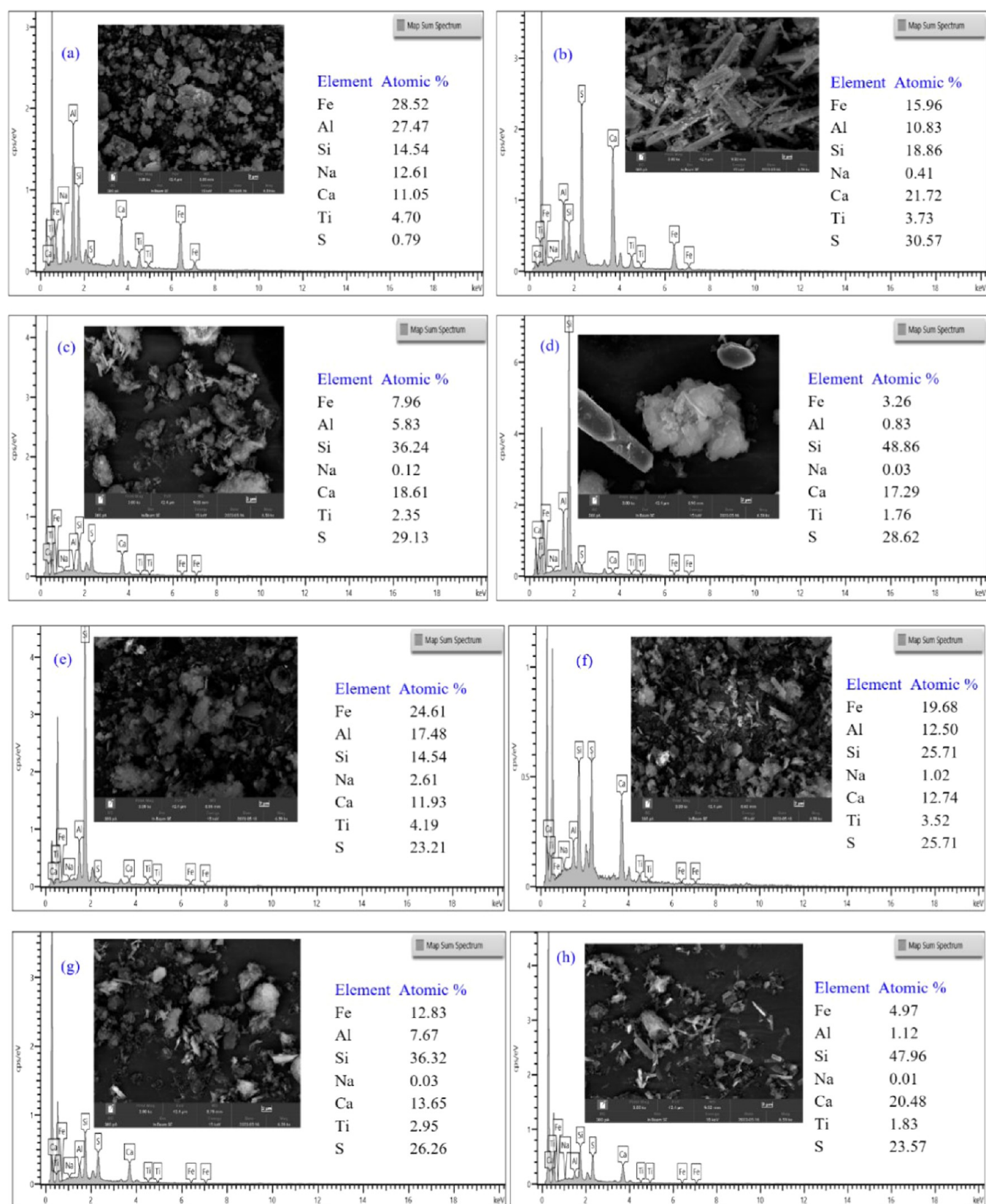


**Figure 4.** SEM analysis of red mud and the acid-leaching residue: (a) red mud, (b) leaching residue with 10% sulfuric acid, (c) leaching residue with 30% sulfuric acid, (d) leaching residue with 50% sulfuric acid, (e) leaching residue at 40 °C, (f) leaching residue at 60 °C, (g) leaching residue at 80 °C, and (h) leaching residue at 100 °C.

temperature, and leaching time increased, the particles of the leaching residue became smaller and dispersed.<sup>36</sup>

According to the element content analysis (Figure 4) and EDS spectrum (Figure 5), the main components of the

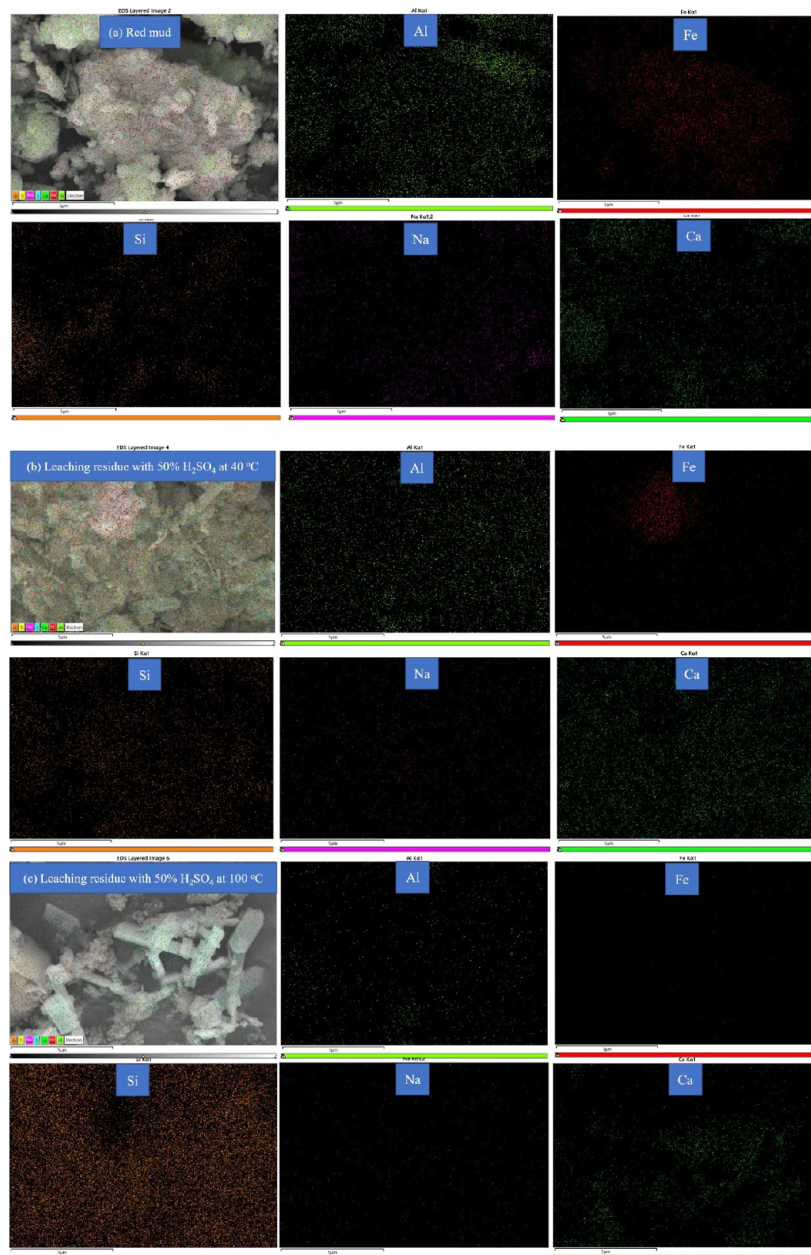


Figure 5. EDS analysis of red mud and the acid-leaching residue.

leaching residue were calcium and silicon. The scattered distribution of aluminum indicated a low content in the leaching residue, which shows that the sulfuric acid leaching process has an obvious effect on the leaching efficiency of aluminum. The distribution of silicon and calcium was both abundant in the leaching residue, indicating that calcium and silicon of red mud were not dissolved into the sulfuric acid solution.

**3.2. Polymerization of Al and Fe in Acid-Leaching Solution.** In the preliminary research process, it was found that the polymerization temperature, time, basicity, and aluminum–iron molar ratio could affect the preparation of aluminum–iron flocculants. The basicity was a key factor, which could change the concentration of hydroxyl ions in the solution system, thereby affecting the polymerization effect of aluminum ions, iron ions, and hydroxyl groups.<sup>37</sup> Finally, the flocculation effect of the flocculant product could also be

affected. Therefore, an investigation on the effect of basicity on the polymerization morphology of aluminum and iron as well as the microstructure of the flocculant product was carried out.

**3.2.1. Dynamic Changes of pH and Species Distribution of Al and Fe.** The dynamic change of the polymerization pH value and the species distribution of Al and Fe in PAFS were studied with different basicities ( $B = 0.3, 0.5, 0.7, 0.9,$  and  $1.1$ ), and the results are shown in Figure 6.

Figure 6a shows that the pH value decreased slightly with an increase of time at a basicity of 0.3. It was due to the low hydrolysis degree of  $\text{Al}^{3+}$  and  $\text{Fe}^{3+}$  with  $\text{OH}^-$  under the condition of low basicity. The mononuclear hydroxyl complex ions of Al and Fe were generated with a basicity range of 0.5–0.9, and the polynuclear hydroxyl complex ions with an oligomerization degree also existed in the mixed solution.<sup>38</sup> The hydroxyl complex ions had good complexation ability to Al and Fe, resulting in further hydrolysis and polymerization.

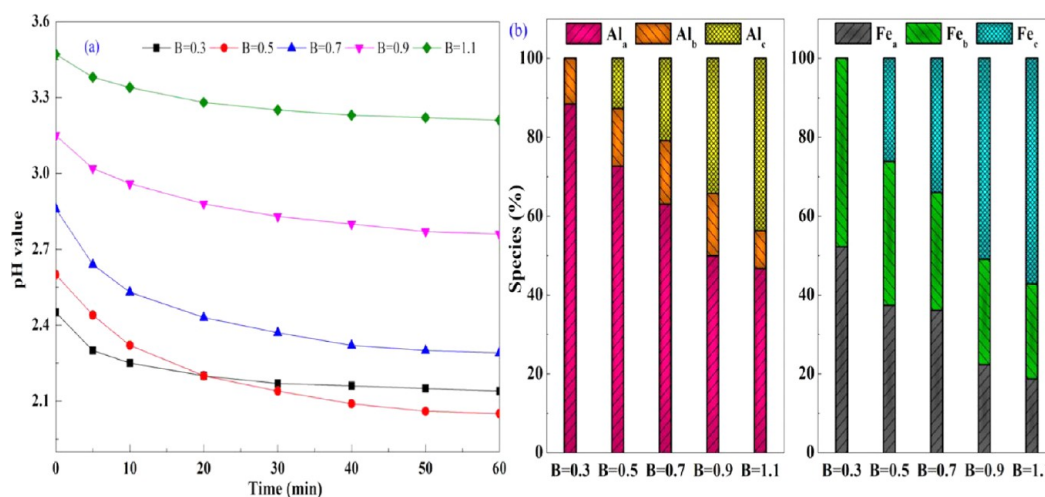


**Figure 6.** Distribution patterns of aluminum and iron in flocculants with different basicities. (a) Dynamic change of the polymerization pH value. (b) Species distribution of Al and Fe.

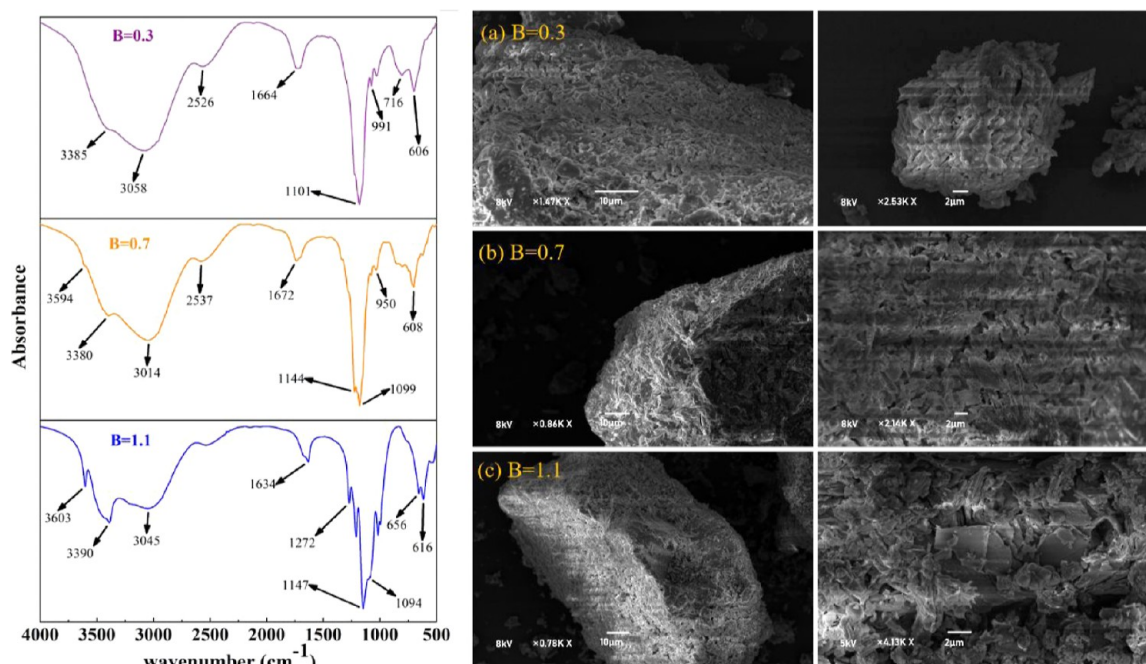


**Figure 7.** FT-IR and SEM for PAFS with different basicities.

Therefore, the high polymers of Al/Fe were very easy to form, which could greatly reduce the pH value.<sup>38,39</sup> The polymerization speed was accelerated with a basicity of 0.9, in which the hydrolysis-saturated state of Al<sup>3+</sup> and Fe<sup>3+</sup> quickly reached and the polymerization mostly existed with the medium and high polymers of Al and Fe. At this time, the complex ability of OH<sup>-</sup> was weakened, and the pH value slightly decreased.<sup>39</sup> Figure 6b shows that the content of Al<sub>a</sub> and Al<sub>c</sub> decreased and increased, respectively, with an increase of basicity. At the same time, the content of the middle polymer decreased with the increase of alkalinity, where the complex ability of polynuclear hydroxyl complex ions to OH<sup>-</sup> was stronger than that of mononuclear hydroxyl complex ions.<sup>40</sup> Therefore, the conversion trend of Al<sub>b</sub>/Fe<sub>b</sub> to precipitated Al<sub>c</sub>/Fe<sub>c</sub> was more obvious with an increase in the basicity. In addition, the content of medium and polymer in the species distribution of Fe(III) was always higher than that of Al(III) under the same

conditions, which was due to the stronger competitiveness to OH<sup>-</sup> of Fe<sup>3+</sup> than that of Al<sup>3+</sup>. OH<sup>-</sup> played a crucial bridging role in the formation of aluminum and iron polymers, which served as a bridge connecting aluminum and iron ions.<sup>39</sup> In addition, compared to iron ions, aluminum ions needed to polymerize with OH<sup>-</sup> at a higher pH value, which was closely related to the form of aluminum and iron ions in solution.<sup>40</sup>

**3.2.2. Structure and Characterization of Polymers.** The FT-IR spectra and SEM analysis of PAFS with different basicities are shown in Figure 7.

The absorption peak of 3000–3700 cm<sup>-1</sup> was produced by stretching, mainly provided by coordination water at low basicity. Two strong hydroxyl stretching vibration peaks of Fe–OH and Al–OH existed in the band of 3600–3390 cm<sup>-1</sup> with an increase of basicity.<sup>41</sup> The result indicates that the hydrolysis degree of Fe<sup>3+</sup> and Al<sup>3+</sup> could be obvious with an increase of basicity. The peak was caused by the stretching

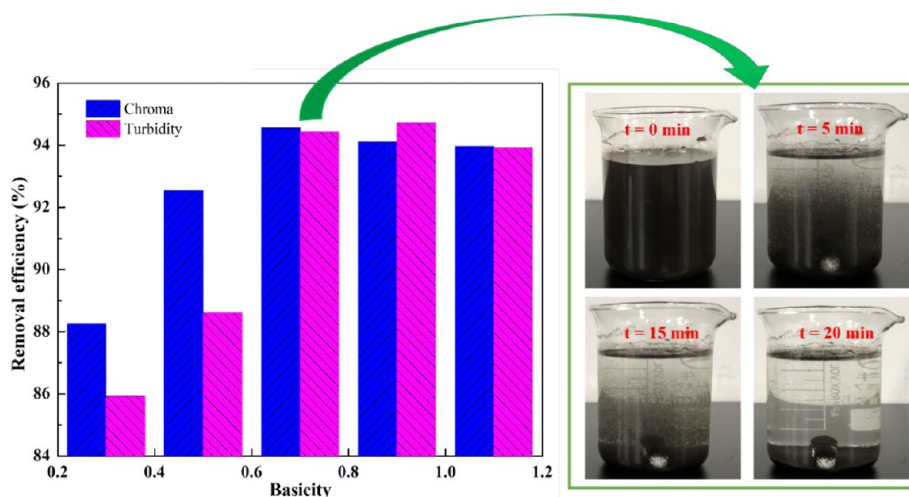


Figure 8. Settling effect of slime water by flocculants with different basicities.

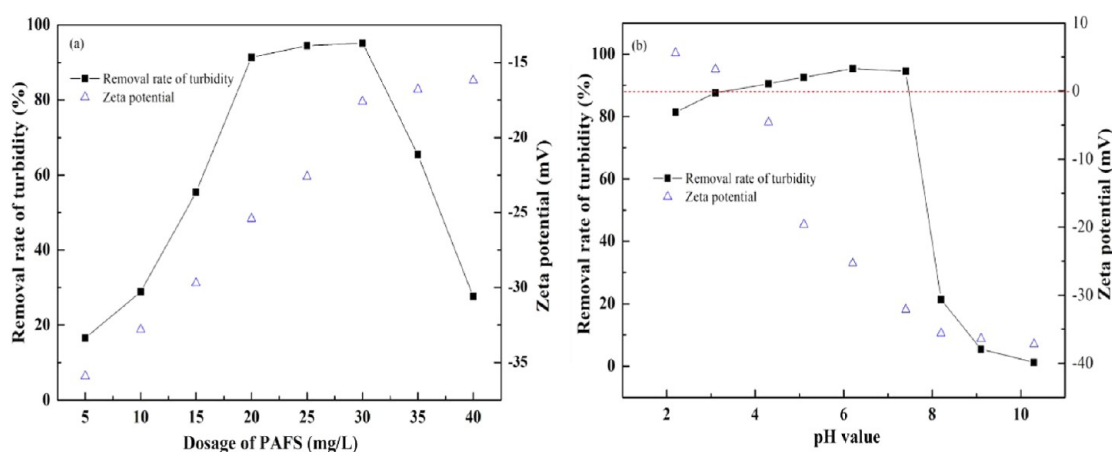


Figure 9. Influence of PAFS dosage (a) and pH value (b).

vibration of Fe–OH–Al at  $2537\text{ cm}^{-1}$  close to the broadband peak of  $3000\text{--}3700\text{ cm}^{-1}$ , which could correspond to the cross copolymer of iron and aluminum.<sup>18</sup> The absorption peak at  $1634\text{--}1672\text{ cm}^{-1}$  was attributed to the bending vibration of H–OH in bound water. Many absorption peaks existed at  $950\text{--}1300\text{ cm}^{-1}$ , which should be the absorption peak of  $\text{SO}_4^{2-}$ .<sup>18,41</sup> There were two strong absorption peaks with the peak of Fe–OH–Fe at  $1100\text{ cm}^{-1}$  and the peak of Al–OH–Al at  $1150\text{ cm}^{-1}$ , respectively.<sup>42</sup> The positions of the two peaks were similar and belonged to the bending vibration of Me–OH on the molecular surface.<sup>43</sup> It shows that both hydroxyl-linked polymeric iron and hydroxyl-bridged polymeric aluminum existed in PAFS. In addition, a vibration absorption peak of Fe–OH–Al also existed. The in-plane bending vibration peaks of Al–OH–Al ( $716\text{ cm}^{-1}$ ) and Fe–OH–Fe ( $606\text{ cm}^{-1}$ ) existed in PAFS. The absorption peak intensities of Al–OH–Al and Fe–OH–Fe increased with an increase of the basicity from 0.3 to 1.1. However, the absorption peak intensity of Al–OH–Al changed more at  $1147$  and  $716\text{ cm}^{-1}$ . It indicates that the hydrolysis of  $\text{Fe}^{3+}$  was carried out at a low basicity, while the hydrolysis degree of  $\text{Al}^{3+}$  was low at the same condition.<sup>44</sup>

The result of SEM shows that the samples of PAFS generally existed as a formless material. The molecular density of PAFS increased, and the structure became more compact with an increase of basicity, which was in accordance with the previous

results.<sup>45</sup> The surface of the aggregate was rough, and the pores were small at a low basicity. The aggregates and the surface became compact and flat, and the pores increased with a basicity of 0.7. However, the aggregate had more pores with a basicity of 1.1, in which the surface became uneven and some disordered crystals grew. The formation of iron hydroxide and aluminum hydroxide was precipitated due to the excessive hydroxyl groups as the alkalinity increased.<sup>46</sup> Overall, the formed PAFS mostly exhibited a chain network structure with many pores at a basicity of 0.7, in which the chain network structure of PAFS extended and interlaced in different directions. A more complex three-dimensional structure was formed in PAFS due to the mutual folding and interlacing of molecular chains. This three-dimensional structure increased the specific surface area and porosity and enhanced the adsorption bridging effect. In the flocculation and purification process of wastewater, it could adsorb colloidal particles in wastewater to form flocculation precipitation and achieve the effect of purifying water.<sup>47</sup>

**3.2.3. Application of PAFS.** PAFS prepared with different basicities have different treatment capacities for turbidity and chroma of wastewater (slime water). The removal efficiency of turbidity and chroma of wastewater by using PAFS with different basicities was studied (see Figure 8).

The changing trend of the removal efficiency on turbidity and chroma of wastewater was similar to an increase in

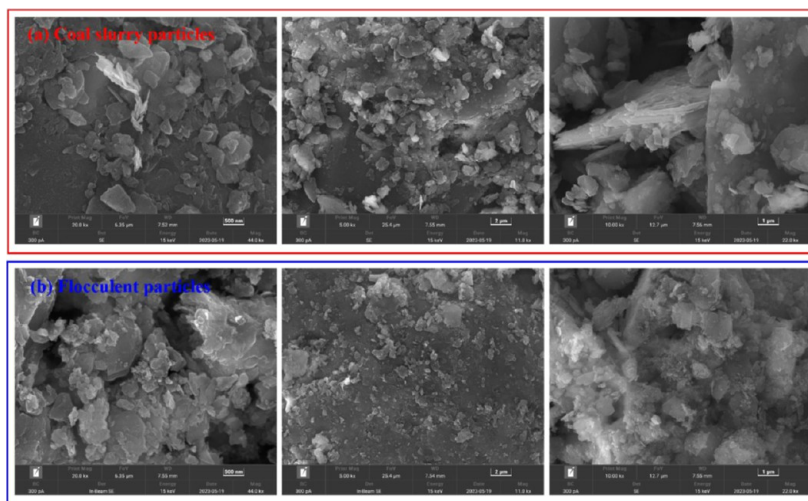


**Figure 10.** SEM patterns of coal slurry particles and flocculent particles.

basicity. The removal efficiency of turbidity and chroma was the highest (95 and 94%) with a basicity of 0.7–0.9. By analyzing the morphological distribution of Al and Fe with different basicities (see Figure 6), there were more oligomers with low basicities (0.3–0.5) in PAFS. The species of  $(\text{Al} + \text{Fe})_a$  played a dominant role under the lower alkalinity conditions. The proportion of polymers formed by aluminum ions and iron ions was relatively small, and most of them existed in the form of ions.<sup>48</sup> Therefore, the removal efficiency of the turbidity was low. The content of medium and high polymers was more with a basicity of 0.7–0.9, in which the species of  $(\text{Al} + \text{Fe})_c$  was dominant, and the removal effect was more obvious. The treatment capacity of wastewater would decrease due to the low content of  $(\text{Al} + \text{Fe})_a$  with high alkalization.<sup>49</sup> A decrease in both turbidity and chromaticity removal efficiencies of the wastewater existed with a basicity of 1.1. It is because a large number of hydroxyl groups in the polymer were generated with high alkalinity. The excessive hydroxyl groups led to the formation of aluminum hydroxide and iron hydroxide precipitates, which could reduce the flocculation performance and stability of PAFS.<sup>50</sup> Therefore, the acid leaching solution of red mud was adjusted to a basicity of 0.7, which was aged and polymerized to prepare PAFS for subsequent wastewater treatment.

The significant effects of flocculants on wastewater treatment were the dosage of the flocculants and the pH value of the wastewater treatment system. The effects of PAFS addition and pH value of the coagulation system on the turbidity removal rate and zeta potential of wastewater were studied at 25 °C for 20 min (see Figure 9).

Figure 9a indicates that the removal effect of turbidity first increased and then decreased with an increase of PAFS dosage from 5 to 40 mg/L. The optimal dosage of the removal range was from 20 to 30 mg/L, and the removal rate of turbidity was from 92.1 to 95.4%. While the dosage was not within this range, the coagulation effect rapidly decreased, and the turbidity removal rate was even lower than 20%. Furthermore, the dosage of PAFS had a significant effect on the zeta potential. The zeta potential gradually increased with an increase of dosage.<sup>51</sup> The zeta potential reached a limit value of  $-17.2$  mV with a PAFS dosage of 30 mg/L, which was gradually stabilized and did not reach the isoelectric point. The coagulation effect of the slime water gradually increased as the

zeta potential of the system was very low, at which point the optimal coagulation area appeared. It indicates that the electric neutralization effect was not the only factor affecting the removal of the turbidity of the slime water by using PAFS. Although PAFS had a large number of positive charges with a low dosage, its effect was negligible relative to the negative electricity of the slime water.<sup>52</sup> So, the enhancement of the coagulation effect may be the effect of other coagulation mechanisms.  $\text{Al}_b$  and  $\text{Fe}_b$  in PAFS formed a special molecular structure, which could adsorb the colloidal particles from coal slime water to grow flocs. Then, the flocs could form larger flocs through the mechanical mesh trapping and sweeping of  $\text{Al}_c$  and  $\text{Fe}_c$ . This inference could also be confirmed by the change in zeta potential, while the dosage continued to increase.<sup>53</sup> The removal effect of turbidity continued to be at a high level for a period of time, while the zeta potential reached stability. However, while the dosage continued to increase (more than 30 mg/L), the removal rate of the turbidity rapidly decreased. It indicates that electroneutralization was not the only action mechanism.<sup>54</sup> Figure 9b shows that the coagulation effect of PAFS in removing the turbidity of coal slurry water was greatly affected by the pH value of the system. The removal effect of turbidity under acidic conditions was better compared with alkaline conditions at the same dosage, in which the removal rate of turbidity was more than 80% at pH values of 2.0–7.0. The coagulation effect was slightly lower with pH 2.0–4.0 than with pH 4.0–7.0. The floc charge changed from positive to negative with a continuing increase of the pH value. The floc charge has reached  $-32.6$  mV at a pH of 7.0, in which the turbidity removal effect of coal slurry water was good and maintained at more than 80% during the change. The turbidity removal rate rapidly decreased to below 20%, and the charge of the floc decreased to below  $-35$  mV at a pH of more than 7.0. The zeta potential gradually reached the isoelectric point, and the coagulation effect reached the optimal value at pH values of 3.0–4.0. This is because the flocs gradually exhibited negative charge, and the prepared PAFS remained relatively stable with a continuous increase of pH value.<sup>55</sup> The network floc particles with high positive charge aggregates still played a dominant role in adsorption, neutralization, and network capture, so the macroscopic performance showed good coagulation (above 90%). The pH value could affect the hydrolysis polymerization behavior of

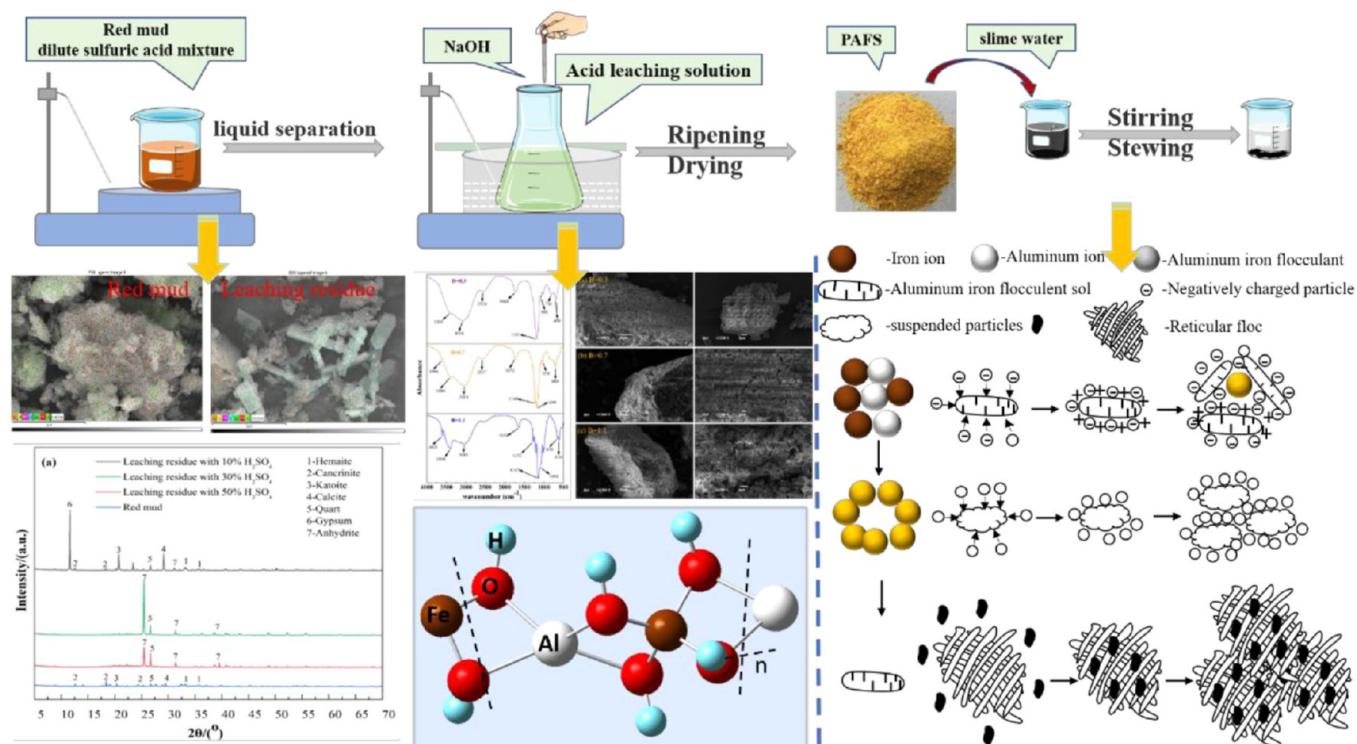


**Figure 11.** Preparation of PASF from red mud and its application to reducing turbidity.

PASF flocculant, which resulted in changes in the forms of  $\text{Al}_b$  and  $\text{Fe}_b$ . The forms of  $\text{Al}_b$  and  $\text{Fe}_b$  were relatively stable under weakly acidic conditions and maintained their original high-charge and molecular-weight forms. Therefore, the effects of charge neutralization, adsorption, network capture, and sweeping were fully exerted to achieve better removal of turbidity in coal slurry water. The partial hydrolysis of  $\text{Al}_b$  and  $\text{Fe}_b$  was inevitable under alkaline conditions (a pH of more than 7.0) and resulted in the formation of  $\text{Al}(\text{OH})_3$  and  $\text{Fe}(\text{OH})_3$ . The coal slurry colloidal particles could not bind with  $\text{Al}(\text{OH})_3$  and  $\text{Fe}(\text{OH})_3$ , so the coagulation effect rapidly decreased without the electric neutralization and destabilization.<sup>56</sup>

PASF was prepared from an acid-leaching solution of red mud with a basicity of 0.7. The slime water was flocculated with a dosage of 30 mg/L and a pH value of 7.0 at 25 °C for 20 min. The coal slurry particles and flocculant particles after flocculation were comparatively analyzed by SEM (Figure 10).

Figure 10 shows that the coal slurry particles in the coal slurry water were very small and did not adhere to each other. The flocs showed mutual folding and interlocking to form a surface after flocculation with PASF. The flocs exhibit an irregular shape with a large number of fine particles adhering to the surface compared to the SEM of PASF in Figure 7. Furthermore, the interior of the flocs was also filled with a large number of fine particles. Therefore, PASF could adsorb the colloidal particles in wastewater during the flocculation and purification processes of coal slurry water. The mechanical trapping could also be formed to further flocculate fine particles and achieve the effect of purifying water, which was consistent with the previous studies.<sup>57</sup> To sum up, the crystal lattice of cancrinite containing aluminum and hematite containing iron in red mud was destroyed by sulfuric acid leaching, in which the main components of aluminum and iron were mostly into the sulfuric acid-leaching solution in the form

of ions. By regulating the basicity of the acid-leaching solution, a yellow flocculant of PASF was obtained after aging and drying at an appropriate temperature, where aluminum, iron, and hydroxyl groups could form different degrees of polymerization of  $\text{Al}_a$ ,  $\text{Al}_b$ ,  $\text{Al}_c$ ,  $\text{Fe}_a$ ,  $\text{Fe}_b$ , and  $\text{Fe}_c$ . The good coagulation effect of slime wastewater was obtained with the flocculant of PASF. There were certain oligomers ( $\text{Al}_a$  and  $\text{Fe}_a$ ) in PASF, where the high valence cation charge could compress the double electric layer of small negatively charged particles in the slime wastewater through electric neutralization. Then, a large number of hydroxyl groups were present in the intermediate polymers ( $\text{Al}_b$  and  $\text{Fe}_b$ ) of PASF, which could adsorb the small particles to gradually grow. Finally, the mechanical trapping effect of high polymers ( $\text{Al}_c$  and  $\text{Fe}_c$ ) in PASF could entrain the floc and form larger flocs to achieve a good reduction effect of turbidity. The mechanism of preparing PASF from red mud and its application in reducing turbidity in coal slurry wastewater are shown in Figure 11.

#### 4. CONCLUSIONS

In this study, the appropriate utilization of red mud based on PASF preparation and application was determined with sulfuric acid leaching, polymerization, and coagulation of coal slurry water. More than 90% aluminum and 60% iron could be leached from red mud under the conditions of a sulfuric acid concentration of 50%, a liquid-to-solid ratio of 7 mL/g, a leaching temperature of 100 °C, and a leaching time of 2 h. The minerals such as cancrinite, calcite, and hematite in the red mud could be significantly destroyed to promote the dissolution of aluminum and iron. The acid-leaching solution was polymerized by adjusting its basicity to 0.7–0.9 to form PASF, in which the molecular density of PASF increased and the structure became more compact with an increase of basicity. The removal efficiency of turbidity and chroma could reach more than 95% by using PASF with 25 mg/L in the pH

range of 6.0–7.0. The reduction of turbidity with PAFS was affected by not only the electric neutralization of low polymer (Al + Fe)<sub>a</sub> but also the adsorption of middle polymer (Al + Fe)<sub>b</sub> and the entrapment of high polymer (Al + Fe)<sub>c</sub>. This study provided the technical support and theoretical basis for the further efficient preparation and application of aluminum iron flocculants from red mud.

## AUTHOR INFORMATION

### Corresponding Authors

**Wang Li** – College of Chemistry and Chemical Engineering, Henan Polytechnic University, Jiaozuo, Henan 454000, China; [orcid.org/0000-0003-4367-4833](https://orcid.org/0000-0003-4367-4833); Phone: +86 391 3986810; Email: [liwang0805@126.com](mailto:liwang0805@126.com)

**Xiaobo Zhu** – College of Chemistry and Chemical Engineering, Henan Polytechnic University, Jiaozuo, Henan 454000, China; Collaborative Innovation Center of Coal Work Safety and Clean High Efficiency Utilization, Jiaozuo, Henan 454000, China; Email: [zhuxiaobo01110@126.com](mailto:zhuxiaobo01110@126.com)

### Author

**Panpan Zhang** – College of Chemistry and Chemical Engineering, Henan Polytechnic University, Jiaozuo, Henan 454000, China

Complete contact information is available at:

<https://pubs.acs.org/10.1021/acsomega.3c07013>

### Notes

The authors declare no competing financial interest.

## ACKNOWLEDGMENTS

The authors gratefully acknowledge the financial support provided by the National Natural Science Foundation of China (51804103 and 51904097), the Key Research and Development Project of Henan Province (231111321800), the Natural Science Foundation of Henan Province (232300420078), the Scientific and Technological Project of Henan Province (232102321138), and the Science Fund for Distinguished Young Scholars of Henan Polytechnic University (J2022-3).

## REFERENCES

- (1) Ma, Q. S.; Fan, F. F. Preparation and applications of red mud-based poly aluminum ferric sulfate. *Shandong Chem. Ind.* **2018**, *47*, 201–203.
- (2) Zhao, Y. L.; Zheng, Y. J.; He, H. B.; Sun, Z. M.; Li, A. Effective aluminum extraction using pressure leaching of bauxite reaction residue from coagulant industry and leaching kinetics study. *J. Environ. Chem. Eng.* **2021**, *9*, 104770.
- (3) Abdila, S. R.; Abdullah, M. M. A. B.; Ahmad, R.; Burduhos Nergis, D. D.; Rahim, S. Z. A.; Omar, M. F.; Sandu, A. V.; Vizureanu, P.; Syafwandi. Potential of soil stabilization using ground granulated blastfurnace slag (GGBFS) and fly ash via geopolymerization method: a review. *Materials* **2022**, *15*, 375.
- (4) Tahir, M. F. M.; Abdullah, M. M. A. B.; Rahim, S. Z. A.; Mohd Hasan, M. R.; Sandu, A. V.; Vizureanu, P.; Ghazali, C. M. R.; Kadir, A. A. Mechanical and durability analysis of fly ash based geopolymer with various compositions for rigid pavement applications. *Materials* **2022**, *15*, 3458.
- (5) Du, D. X.; Xu, C. Y.; Liu, W. Y.; Sun, H. T.; Guo, Y. J.; Wu, W. R.; Tang, Q. J. Application and research status of red mud in wastewater treatment. *Technol. Dev. Chem. Ind.* **2021**, *50*, 55–58.
- (6) Lallemand, C.; Ambrosi, J. P.; Borschneck, D.; Angeletti, B.; Chaurand, P.; Campos, A.; Desmau, M.; Fehlauer, T.; Auffan, M.; Labille, J.; Roche, N.; Poizat, L.; Collin, B.; Rose, J.; Levard, C. Potential of Ligand-Promoted Dissolution at Mild pH for the Selective Recovery of Rare Earth Elements in Bauxite Residues. *ACS Sustainable Chem. Eng.* **2022**, *10*, 6942–6951.
- (7) Kong, Y. L.; Ma, Y. Q.; Ding, L.; Ma, J. Y.; Zhang, H. W.; Chen, Z. L.; Shen, J. M. Coagulation behaviors of aluminum salts towards humic acid: Detailed analysis of aluminum speciation and transformation. *Sep. Purif. Technol.* **2021**, *259*, 118137.
- (8) Li, X. L.; Liang, Y. L.; Deng, L. X.; Xin, L. Study on treatment of wastewater containing Cr (VI) with polymeric phosphate aluminum-ferric chloride coagulant. *Ind. Water Treat.* **2021**, *41*, 101–105.
- (9) Wang, X.; Zhang, G.; Li, L. F.; Wang, W. X.; Feng, W. L.; Li, B. R. Study on preparation technology of polyaluminum ferric chloride in flocculant. *Coal Chem. Ind.* **2020**, *43*, 137–140.
- (10) Rajala, K.; Gronfors, O.; Hesampour, M.; Mikola, A. Removal of microplastics from secondary wastewater treatment plant effluent by coagulation/flocculation with iron, aluminum and polyamine-ferrous chemicals. *Water Res.* **2020**, *183*, 116045.
- (11) Zhu, G. C.; Zheng, H. L.; Chen, W. Y.; Fan, W.; Zhang, P.; Tshukudu, T. Preparation of a composite coagulant: Polymeric aluminum ferric sulfate (PAFS) for wastewater treatment. *Desalination* **2012**, *285*, 315–323.
- (12) Zhao, C. L.; Zhou, J. Y.; Yan, Y.; Yang, L. W.; Xing, G. H.; Li, H. Y.; Wu, P.; Wang, M. Y.; Zheng, H. L. Application of coagulation/flocculation in oily wastewater treatment: A review. *Sci. Total Environ.* **2021**, *765*, 142795.
- (13) Prokopova, M.; Novotna, K.; Pivokonska, L. K.; Cermakova, L. K.; Cajthaml, T.; Pivokonsky, M. Coagulation of polyvinyl chloride microplastics by ferric and aluminium sulphate: Optimisation of reaction conditions and removal mechanisms. *J. Environ. Chem. Eng.* **2021**, *9*, 106465.
- (14) de Oliveira Anício, S.; dos Santos Lopes, V.; de Oliveira, A. L. PSD and fractal dimension for flocculation with different parameters and ferric chloride, aluminium polychloride and aluminium sulfate as coagulants. *J. Water Process Eng.* **2021**, *43*, 102180.
- (15) Zhao, R.; Liu, Z. A.; Chang, Y.; Liu, Q. W. Preparation of PAFS cationic flocculant in various Fe<sup>3+</sup>/Al<sup>3+</sup> molar ratio. *J. Inn. Mong. Norm. Univ., Nat. Sci. Ed.* **2011**, *40*, 508–511.
- (16) Zhang, H. H.; Lin, H.; Li, Q.; Cheng, C. K.; Shen, H.; Zhang, Z. Y.; Zhang, Z. Z.; Wang, H. M. Removal of refractory organics in wastewater by coagulation/flocculation with green chlorine-free coagulants. *Sci. Total Environ.* **2021**, *787*, 147654.
- (17) Sun, C. Z.; Yue, Q. Y.; Gao, B. Y.; Cao, B. H.; Mu, R. M.; Zhang, Z. B. Synthesis and flocculation properties of polymeric ferric aluminum chloride-polydimethyl diallylammonium chloride coagulant in coagulating humic acid-kaolin synthetic water. *Chem. Eng. J.* **2012**, *185–186*, 29–34.
- (18) Zhu, G. C.; Zheng, H. L.; Zhang, Z.; Tshukudu, T.; Zhang, P.; Xiang, X. Y. Characterization and coagulation-flocculation behavior of polymeric aluminum ferric sulfate (PAFS). *Chem. Eng. J.* **2011**, *178*, 50–59.
- (19) Luo, J. Q.; Wang, L. L.; Li, Q. S.; Zhang, Q. K.; He, B. Y.; Wang, Y.; Qin, L. P.; Li, S. S. Improvement of hard saline-sodic soils using polymeric aluminum ferric sulfate (PAFS). *Soil Tillage Res.* **2015**, *149*, 12–20.
- (20) Liang, J. L.; Gu, H. Q.; Zhang, S. W.; Huang, J. J.; Ye, M. Y.; Yang, X.; Li, S. P.; Huang, S. S.; Sun, S. Y. Novel insight into sludge dewaterability mechanism using polymeric aluminium ferric chloride and anaerobic mesophilic digestion treatment under ultrahigh pressure condition. *Sep. Purif. Technol.* **2020**, *234*, 116137.
- (21) Zhuang, J.; Qi, Y. H.; Yang, H. Z.; Li, H. Y.; Shi, T. H. Preparation of polyaluminum zirconium silicate coagulant and its performance in water treatment. *J. Water Process Eng.* **2021**, *41*, 102023.
- (22) Xu, M.; Luo, Y. X.; Wang, X. M.; Zhou, L. X. Coagulation-ultrafiltration efficiency of polymeric Al, Fe, and Ti coagulant with or without polyacrylamide composition. *Sep. Purif. Technol.* **2022**, *280*, 119957.
- (23) Ding, S. H.; Zhou, J. M.; Zhang, M. Y.; Liu, Y. Q.; Fu, Y. S. Experimental study on preparation and application of polymeric

- aluminum ferric calcium chloride from coal gangue. *J. Civ. Environ. Eng.* **2021**, *43*, 185–194.
- (24) Gao, H. L.; Hu, J. Z.; Guo, L.; Li, H. T.; Zhang, G. W.; Zhang, L. Stability of fly ash based polysilicate aluminum ferric flocculant. *Coal Sci. Technol.* **2020**, *48*, 236–241.
- (25) Lu, F. H. Preparing of PFAC with Bayer red mud and hydrochloric acid and treating industrial wastewater. *Hydrometall. China* **2015**, *34*, 79–82.
- (26) Qian, Y.; Zhou, S. J. Synthesis of PAFS based on red mud and its flocculation capacity assessment. *Environ. Eng.* **2016**, *34*, 6–10.
- (27) Bang, K. H.; Kang, Y. B. Recycling red mud to develop a competitive desulfurization flux for kanbara reactor (KR) desulfurization process. *J. Hazard. Mater.* **2022**, *440*, 129752.
- (28) Li, W. Y.; Wang, N.; Lu, F. H.; Chai, H. Y.; Gu, H. N. Selective separation of aluminum, silicon, and titanium from red mud using oxalic acid leaching, iron precipitation and pH adjustments with calcium carbonate. *Hydrometallurgy* **2024**, *223*, 106221.
- (29) Hu, G.; Lyu, F.; Khoso, S. A.; Zeng, H.; Sun, W.; Tang, H. H.; Wang, L. Staged leaching behavior of red mud during dealcalization with mild acid. *Hydrometallurgy* **2020**, *196*, 105422.
- (30) Zhu, X. B.; Niu, Z. P.; Li, W.; Zhao, H.; Tang, Q. J. A novel process for recovery of aluminum, iron, vanadium, scandium, titanium and silicon from red mud. *J. Environ. Chem. Eng.* **2020**, *8*, 103528.
- (31) Zhu, P. W.; Dai, H.; Han, L.; Xu, X. L.; Cheng, L. M.; Wang, Q. H.; Shi, Z. L. Aluminum extraction from coal ash by a two-step acid leaching method. *J. Zhejiang Univ., Sci., A* **2015**, *16*, 161–169.
- (32) Sangita, S.; Nayak, N.; Panda, C. R. Extraction of aluminium as aluminium sulphate from thermal power plant fly ashes. *Trans. Nonferrous Met. Soc. China* **2017**, *27*, 2082–2089.
- (33) Xiao, J.; Li, F. C.; Zhong, Q. F.; Bao, H. G.; Wang, B. J.; Huang, J. D.; Zhang, Y. B. Separation of aluminum and silica from coal gangue by elevated temperature acid leaching for the preparation of alumina and SiC. *Hydrometallurgy* **2015**, *155*, 118–124.
- (34) Pepper, R. A.; Couperthwaite, S. J.; Millar, G. J. Comprehensive examination of acid leaching behaviour of mineral phases from red mud: Recovery of Fe, Al, Ti, and Si. *Miner. Eng.* **2016**, *99*, 8–18.
- (35) Wu, Y. H. Z.; Zhou, K. G.; Zhang, X. K.; Peng, C. H.; Jiang, Y.; Chen, W. Aluminum separation by sulfuric acid leaching-solvent extraction from Al-bearing LiFePO<sub>4</sub>/C powder for recycling of Fe/P. *Waste Manage.* **2022**, *144*, 303–312.
- (36) Wu, C. Y.; Yu, H. F.; Zhang, H. F. Extraction of aluminum by pressure acid-leaching method from coal fly ash. *Trans. Nonferrous Met. Soc. China* **2012**, *22*, 2282–2288.
- (37) Sun, Y. J.; Shah, K. J.; Sun, W. Q.; Zheng, H. L. Performance evaluation of chitosan-based flocculants with good pH resistance and high heavy metals removal capacity. *Sep. Purif. Technol.* **2019**, *215*, 208–216.
- (38) Sousa, A. F. D.; Braga, T. P.; Gomes, E. C. C.; Valentini, A.; Longhinotti, E. Adsorption of phosphate using mesoporous spheres containing iron and aluminum oxide. *Chem. Eng. J.* **2012**, *210*, 143–149.
- (39) Peng, H. L.; Zhong, S. X.; Xiang, J. X.; Lin, Q. T.; Yao, C.; Dong, J. H.; Yin, G. C.; Yao, K.; Zeng, S. Y.; Zhong, J. Characterization and secondary sludge dewatering performance of a novel combined aluminum-ferrous-starch flocculant (CAFS). *Chem. Eng. Sci.* **2017**, *173*, 335–345.
- (40) Lin, Q. T.; Peng, H. L.; Zhong, S. X.; Xiang, J. X. Synthesis, characterization, and secondary sludge dewatering performance of a novel combined silicon-aluminum-iron-starch flocculant. *J. Hazard. Mater.* **2015**, *285*, 199–206.
- (41) Sun, Y. J.; Yu, Y. Y.; Liang, Y. K.; Sun, W. Q.; Shah, K. J.; Zheng, H. L. Flocculation performance of PCFA composite coagulant for removing nanoparticles. *Colloids Surf., A* **2023**, *673*, 131828.
- (42) Ma, J.; Wang, R. N.; Wang, X. Y.; Zhang, H.; Zhu, B.; Lian, L. L.; Lou, D. W. Drinking water treatment by stepwise flocculation using polysilicate aluminum magnesium and cationic polyacrylamide. *J. Environ. Chem. Eng.* **2019**, *7*, 103049.
- (43) Kajjumba, G. W.; Fischer, D.; Risso, L.; Koury, D.; Marti, E. Application of cerium and lanthanum coagulants in wastewater treatment-A comparative assessment to magnesium, aluminum, and iron coagulants. *Chem. Eng. J.* **2021**, *426*, 131268.
- (44) Ding, C. J.; Xie, A.; Yan, Z.; Li, X. Y.; Zhang, H. F.; Tang, N.; Wang, X. C. Treatment of water-based ink wastewater by a novel magnetic flocculant of boron-containing polysilicic acid ferric and zinc sulfate. *J. Water Process Eng.* **2021**, *40*, 101899.
- (45) Zheng, H.; Jiang, Z.; Zhu, J.; Tan, M.; Feng, L.; Liu, L.; Chen, W. Study on structural characterization and algae-removing efficiency of polymeric aluminum ferric sulfate (PAFS). *Desalin. Water Treat.* **2013**, *51*, 5674–5681.
- (46) Ordaz-Diaz, L. A.; Valle-Cervantes, S.; Rodriguez-Rosales, J.; Bailon-salas, A. M.; Madrid-Del Palacio, M.; Torres-Fraga, K.; De la Peña-Arellano, L. A. Zeta Potential as a tool to evaluate the optimum performance of a coagulation-flocculation process for wastewater internal treatment for recirculation in the pulp and paper process. *Bioresources* **2017**, *12*, 5953–5969.
- (47) López-Maldonado, A.; Oropeza-Guzmán, M. T.; Ochoa-Terán, A. Improving the efficiency of a coagulation-flocculation wastewater treatment of the semiconductor industry through Zeta potential measurements. *J. Chem.* **2014**, *2014*, 969720.
- (48) Guo, K. Y.; Gao, Y.; Gao, B. Y.; Feng, Q. Y.; Shen, X.; Liu, C. Y.; Yue, Q. Y.; Xu, X. Structure-activity relationships of the papermill sludge-based flocculants in different dye wastewater treatment. *J. Cleaner Prod.* **2020**, *266*, 121944.
- (49) Cao, B.; Gao, B.; Wang, M.; Sun, X.; Wang, J. Flocculation properties of polyaluminum ferric chloride in water treatment: the effect of Al/Fe molar ratio and basicity. *J. Colloid Interface Sci.* **2015**, *458*, 247–254.
- (50) Gerchman, Y.; Vasker, B.; Tavasi, M.; Mishael, Y.; Kinel-Tahan, Y.; Yehoshua, Y. Effective harvesting of microalgae: Comparison of different polymeric flocculants. *Bioresour. Technol.* **2017**, *228*, 141–146.
- (51) Li, H. L.; Chen, J.; Peng, C. L.; Min, F. F.; Song, S. X. Salt coagulation or flocculation? In situ zeta potential study on ion correlation and slime coating with the presence of clay: A case of coal slurry aggregation. *Environ. Res.* **2020**, *189*, 109875.
- (52) Wang, M.; Muhammed, M. Novel synthesis of Al<sub>13</sub>-cluster based alumina minerals. *Nanostruct. Mater.* **1999**, *11*, 1219–1229.
- (53) Sabah, E.; Erkan, Z. E. Interaction mechanism of flocculants with coal waste slurry. *Fuel* **2006**, *85*, 350–359.
- (54) Duan, J. M.; Wang, J. H.; Graham, N.; Wilson, F. Coagulation of humic acid by aluminium sulphate in saline water conditions. *Desalination* **2002**, *150*, 1–14.
- (55) Yan, M. Q.; Wang, D. S.; Qu, J. H.; He, W. J.; Chow, C. W. K. Relative importance of hydrolyzed Al(III) species (Al<sub>3</sub>, Al<sub>2</sub>, and Al<sub>1</sub>) during coagulation with polyaluminum chloride: A case study with the typical micro-polluted source waters. *J. Colloid Interface Sci.* **2007**, *316*, 482–489.
- (56) Pandey, A.; Pathak, V. V.; Kothari, R.; Black, P. N.; Tyagi, V. V. Experimental studies on zeta potential of flocculants for harvesting of algae. *J. Environ. Manage.* **2019**, *231*, 562–569.
- (57) Zhang, Z. Q.; Xia, S. Q.; Zhao, J. F.; Zhang, J. Characterization and flocculation mechanism of high efficiency microbial flocculant TJ-F1 from *Proteus mirabilis*. *Colloids Surf., B* **2010**, *75*, 247–251.